Eulerian Particle Flamelet Modeling for Combustion Processes of Bluff-Body Stabilized Methanol-Air Turbulent Nonpremixed Flames

Seong-Ku Kim
Korea Aerospace Research Institute, Daejeon, Korea
Sungmo Kang, Yongmo Kim*
Department of Mechanical Engineering, Hanyang University, 17, Haengdang-Dong, Sungdong-Ku, Seoul 133-791, Korea

The present study is focused on the development of the RIF (Representative Interactive Flamelet) model which can overcome the shortcomings of conventional approach based on the steady flamelet library. Due to the ability for interactively describing the transient behaviors of local flame structures with CFD solver, the RIF model can effectively account for the detailed mechanisms of NOx formation including thermal NO path, prompt and nitrous NOx formation, and reburning process by hydrocarbon radical without any ad-hoc procedure. The flamelet time of RIFs within a stationary turbulent flame may be thought to be Lagrangian flight time. In context with the RIF approach, this study adopts the Eulerian Particle Flamelet Model (EPFM) with mutiple flamelets which can realistically account for the spatial inhomogeneity of scalar dissipation rate. In order to systematically evaluate the capability of Eulerian particle flamelet model to predict the precise flame structure and NO formation in the multi-dimensional elliptic flames, two methanol bluffbody flames with two different injection velocities are chosen as the validation cases. Numerical results suggest that the present EPFM model has the predicative capability to realistically capture the essential features of flame structure and NOx formation in the bluff-body stabilized flames.

Key Words: Turbulent Nonpremixed Bluffbody Flames, Eulerian Particle Flamelet Model, Turbulent-chemistry Interaction, Full NOx Chemistry, Radiation

Nomenclature

$a_{p,k}$: Planck mean absorption coefficient for radiating species k
c_p : Specific heat of mixture at constant pressure
D_i : Diffusion coefficient of species i
d : Fuel nozzle diameter
h, h_k : Enthalpy of mixture and species k
P : Probability density function
Y_i : Mass fraction of species i
Z : Mixture fraction

Greek Symbols

ρ : Density
σ_B : Stefan-Boltzmann constant
$\dot{\omega}_k$: Chemical production rate of species k

Subscripts

χ : Scalar dissipation rate
st : Stoichiometry

Superscripts

$\overline{\phi}$: Reynolds-averaged (density-unweighted)
$\widetilde{\phi}$: Favre-averaged (density-weighted)

* Corresponding Author,
E-mail : ymkim@hanyang.ac.kr
TEL : +82-2-2220-0428; **FAX** : +82-2-2297-0339
Department of Mechanical Engineering, Hanyang University, 17, Haengdang-Dong, Sungdong-Ku, Seoul 133-791, Korea. (Manuscript **Received** August 17, 2005; **Revised** May 30, 2006)

1. Introduction

For the numerical study of fundamental processes involved in nonpremixed turbulent combustion, the laminar flamelet concept, the CMC (conditional moment closure) model, and the PDF (probability density function) transport model have been emerged as the promising tools for simulating the turbulent reacting flows. Although these turbulent combustion models have its own superiority over each other and their prediction capabilities have been incessantly improved, the present review on the previous works is focused on the recent progress in the flamelet modeling. However, it will be very worthwhile to refer to the recently published review papers (Klimenko and Bilger, 1999 ; Vervisch and Veynante, 2002) and textbooks (Libby and Williams, 1994 ; Peters, 2000 ; Pope, 2000) for understanding the accomplishments and both differences and interlinks among these models.

The modeling based on laminar flamelet concept has been widely used during the last two decades, and recently, broadened successfully the applicable capabilities to various combustion problems such as simple jet flames (Ferreira, 1996 ; Marracino and Lentini, 1997 ; Kim and Kim, 2002), gas turbine engine and furnace (Barths et al., 1998 ; Coelho and Peters, 2001), diesel spray combustion (Pitsch et al., 1996 ; Barths et al., 2000), and partially premixed flames (Chen et al., 2000 ; Kim et al., 2004a). The growing attentions to the flamelet modeling are mainly due to the effective incorporation of complex combustion phenomena such as detailed chemical kinetics, differential diffusion, and soot formation by decoupling from the turbulent flow and mixture fraction fields.

The common idea of flamelet models is to view the local flame structure of turbulent flame as an ensemble of laminar flamelets, which are stretched and wrinkled by turbulent flows. Most of the previous works using the flamelet models have relied on the steady state assumption of the flamelets, which allows the construction of the flamelet library by solving steady flamelet equations prior to a CFD calculation. However, there are the certain circumstances where the steady state flamelet assumption is not valid, and the emerging research works have recently been performed to overcome this shortcoming. For essentially unsteady phenomena, such as the local extinction and reignition processes in lifted flames and auto-ignition of sprays, the conventional "flamelet library" approach is not appropriate any more since flamelets do not respond infinitely fast to the changes of the flow field. To analyze the local extinction and reignition associated with the flame stabilization mechanism, Ferreira (1996) has proposed an unsteady flamelet model in which transient effect is taken into account by introducing two additional parameters such as characteristic flame time and reaction progress variable into the steady flamelet library. For simulation of the transient spray combustion where the formation of the mixture field due to evaporation occurs very rapidly and leads to strong mixture fraction gradients, Pitsch et al.(1996) developed the so called RIF (Representative Interactive Flamelet) concept in which the flamelet equations are solved interactively within CFD solver instead of the use of steady flamelet library. The RIF model has been successfully applied to predict the auto-ignition, partially premixed burning, diffusive combustion and pollutant formation like NOx and soot because these complex phenomena related to the detailed chemical kinetics need not to be modeled separately, but are part of the comprehensive chemical mechanism.

The important progress in flamelet modeling has been made for the unsteady flamelet model in a stationary turbulent nonpremixed jet flame. Pitsch et al.(1998) have shown that it is important to describe the transient behavior of the flamelet if slow processes such as NOx formation and radiation are involved, and proposed an unsteady flamelet approach which treats the streamwise evolution of local flame structure in a Lagrangian like sense and this model is often called the Lagrangian Flamelet Model (LFM). The slow processes such as NOx formation and radiation are conflicted with the steady state assumption of flamelet, and the additional treatments in the steady flamelet procedure are needed to realistically rep-

resent such slow processes. For examples, the steady flamelet model generally requires a post-processing step with modeling the time averaged NO formation rate. The Lagrangian flamelet model is able to incorporate the NOx chemistry directly into flamelet equations, and therefore allows the detailed analysis of NOx formation mechanisms including thermal NO path, prompt and nitrous NOx formation, and reburn by hydrocarbon radicals. On the other hand, these detailed NOx formation mechanisms are hardly taken into account in the steady flamelet approach. The application of the unsteady flamelet model can be extended to numerically investigate differential diffusion (Pitsch, 2000) and soot formation (Pitsch et al., 2000) in the turbulent jet diffusion flames. Recently Pitsch and Steiner (2000) have applied the unsteady flamelet model in a large-eddy simulation of a piloted partially premixed flame. However, this Lagrangian flamelet model is only applicable to the parabolic flame fields such as jet flames because the flamelet time and spatial distribution have to be presumed that the local flame structure is a function only of axial distance from the fuel nozzle. In order to overcome this limitation of Lagrangian flamelet model, Barths et al.(1998) have proposed the more general model by introducing an Eulerian equation for the probability to find the multiple flamelets, which is also applied to the transient gaseous and spray combustion problems (Kim et al., 2004b; Barths et al., 2000). In the frame of the EPF model, each flamelet is represented by a fictitious marker particle, and each cell of computational domain does not belong to one flamelet but belongs to several flamelets. This Eulerian particle flamelet model can realistically account for the spatial inhomogeneity of scalar dissipation rate. They have applied the Eulerian particle flamelet model to simulate NOx and soot formation in the elliptic flame fields including a gas turbine combustor. Recently, Coelho and Peters (2001) have applied the EPF model to a methane-air piloted jet flame and a low-flow-rate burner operating in the MILD combustion mode. However, the extensive study has not been carried out for evaluating the predictive performance of the EPF models, especially for the local flame structures which are represented mathematically by conditional means of scalars.

In context with the RIF approach, this study adopts the Eulerian Particle Flamelet Model (EPFM) with mutiple flamelets which can realistically account for the spatial inhomogeneity of scalar dissipation rate. In order to systematically evaluate the capability of Eulerian particle flamelet model to predict the precise flame structure and NO formation in the multi-dimensional elliptic flames, two methanol bluff-body flames with two different injection velocities are chosen as the validation cases. Based on numerical results obtained by the Eulerian particle flamelet model, the detailed discussions have been made for the turbulence-chemistry interaction, radiation effect, and the limitations of the present model.

2. Physical and Numerical Models

2.1 Flamelet equations

Peters (1986) derived the flamelet equations for each chemical species and energy under introducing a coordinate system attached to the surface of stoichiometric mixture. Recently these flamelet equations have been derived by using a two-scale asymptotic analysis (Peters, 2000).

$$\frac{\partial Y_i}{\partial t}=\frac{\chi}{2}\frac{\partial^2 Y_i}{\partial Z^2}+\frac{\dot{\omega}_i}{\rho} \tag{1}$$

$$\frac{\partial T}{\partial t}=\frac{\chi}{2}\frac{1}{c_p}\frac{\partial^2 h}{\partial Z^2}-\frac{\chi}{2}\frac{1}{c_p}\sum_{k=1}^{N}h_k\frac{\partial^2 Y_k}{\partial Z^2}-\frac{1}{\rho c_p}\left(\sum_{k=1}^{N}h_k\dot{\omega}_k-\frac{\partial p}{\partial t}+\nabla\cdot q_{rad}\right) \tag{2}$$

These flamelet equations describe the instantaneous local structure of the flame sheet accounting for nonequilibrium by stretch. In these expressions, the differential diffusion terms are neglected. The radiation heat loss in Eq. (2) is represented by the optically thin model. With the assumption of the optically thin limit, the radiative loss rate per unit volume can be expressed as:

$$\nabla\cdot q_{rad}(T, Y_k)=4\sigma_B(T^4-T_b^4)\sum P_k\cdot a_{p,k} \tag{3}$$

where σ_B is the Stefan-Boltzmann constant, P_k the partial pressure of species k, T the local flame

temperature and T_b the background temperature. The Planck mean absorption coefficients $a_{p,k}$ for radiating species k such as H_2O, CO, and CO_2 are calculated from the curve fits recommended by TNF workshop which has been correctly updated at June, 2000 (Web page for the International Workshop on Measurement and Computation of Turbulent Nonpremixed Flames, www.ca.sandia.gov/tdf/Workshop.html).

The influence of the scalar dissipation rate χ on the structure of diffusion flames was extensively discussed by Peters (1986). In general, the scalar dissipation rate at the stoichiometric mixture fraction governs the departure from chemical equilibrium. In the flamelet modeling procedure, the relation between the scalar dissipation rate and the mixture fraction is needed. Pitsch (2000) has proposed the following one-parametric function for the dependence of scalar dissipation rate on mixture fraction by considering one-dimensional semi-infinite mixing layer.

$$\chi(Z) \equiv 2D_Z\left(\frac{\partial Z}{\partial x_j}\right)^2 \cong \chi_{st} f(Z) = \chi_{st}\frac{Z^2}{Z_{st}^2}\frac{\ln Z}{\ln Z_{st}} \quad (4)$$

Since this model has demonstrated the reasonably good performance in terms of accuracy and efficiency, the present study has utilized this relation for modeling the conditional averaged scalar dissipation rate. However, it is necessary to note that this model is not consistent with the pdf transport equation for the mixture fraction and this might be a source of potential error. In the large eddy simulation of a turbulent piloted methane/air diffusion flame using the Lagrangian flamelet model, Pitsch and Steiner (2000) have proposed a new direct modeling of conditional scalar dissipation rate which needs no longer the prescription of the functional dependence such as Eq. 4 and can account for the influence of local deviations from a simple mixing layer structure. On the other hand, Kronenburg et al.(2000) suggested a new model which is consistent with the pdf transport equation for the mixture fraction and is capable of accounting for non-homogeneities in the flame field. In this aspect, the further study is needed to clarify the issues in modeling the conditional averaged scalar dissipation rate.

2.2 Eulerian particle flamelet model using multiple RIF concept

In context with the transient flamelet models, the use of Lagrangian flamelet approach is limited only to the parabolic flame fields such as jet flames because the flamelet time and spatial distribution have to be presumed that the local flame structure is a function only of axial distance from the fuel nozzle. In the frame of the EPFM, on the other hand, different flamelet histories can be calculated under this model, and each cell of computational domain does not belong to one flamelet but belongs to several flamelets. Each flamelet is represented by a fictitious marker particle, and the probability to find l_{th} particle at location x and time t is given by a convective-diffusive Eulerian equation.

$$\frac{\partial}{\partial t}(\bar{\rho}\tilde{I}_l) + \frac{\partial}{\partial x_j}(\bar{\rho}\tilde{u}_j\tilde{I}_l) = \frac{\partial}{\partial x_j}\left(\frac{\mu_{eff}}{\sigma_I}\frac{\partial \tilde{I}_1}{\partial x_j}\right) \quad (5)$$

where $\tilde{I}_l(\mathbf{x}, t)$ is the probability that l_{th} flamelet can be found in the cell at location x at time t.

Considering the distribution of several flamelets, the local species mass fractions are calculated using the following equation:

$$\tilde{Y}_k(\mathbf{x}, t) = \sum_{l=1}^{N_l}\tilde{I}_l(\mathbf{x}, t)\int_0^1 Y_k^l(Z, \langle\chi/Z\rangle_l;\, t)\,\tilde{P}(Z;\, \mathbf{x}, t)\,dZ \quad (6)$$

At a given time t, the surface-averaged scalar dissipation rate of the l_{th} flamelet at stoichiometry is computed by converting the surface integrals into volume integrals and weighting with the probability of the occurrence of l_{th} particle:

$$\langle\hat{\chi_{st}}\rangle_l(t) = \frac{\int_V \tilde{I}_l(\mathbf{x}, t)\,\bar{\rho}(\mathbf{x}, t)\,[\langle\chi_{st}\rangle(\mathbf{x}, t)]^{3/2}\tilde{P}(Z_{st};\, \mathbf{x}, t)\,dV'}{\int_V \tilde{I}_l(\mathbf{x}, t)\,\bar{\rho}(\mathbf{x}, t)\,[\langle\chi_{st}\rangle(\mathbf{x}, t)]^{1/2}\tilde{P}(Z_{st};\, \mathbf{x}, t)\,dV'} \quad (7)$$

More detailed description of EPFM model can be also found in the recent work of Barths et al. (2000).

In transient spray combustion, RIFs in context with EPFM model are thought to undergo the change of flow and mixing field according to the real time of problem. On the other hand, in the

stationary flame field, RIFs are introduced through the fuel nozzle. In other words, the flamelet of RIFs in transient combustion problem can be taken as the physical time whereas that of RIFs within a stationary turbulent flame may be thought to be Lagrangian flight time. Because the flow and mixture fields are steady, equation (7) can be rewritten as

$$\langle\widehat{\chi_{st}}\rangle_l(t) = \frac{\int_V \tilde{I}_l(\mathbf{x},t)\,\bar{\rho}(\mathbf{x})\,[\langle\chi_{st}\rangle(\mathbf{x})]^{3/2}\tilde{P}(Z_{st};\mathbf{x})\,dV'}{\int_V \tilde{I}_l(\mathbf{x},t)\,\bar{\rho}(\mathbf{x})\,[\langle\chi_{st}\rangle(\mathbf{x})]^{1/2}\tilde{P}(Z_{st};\mathbf{x})\,dV'} \quad (8)$$

Therefore, the temporal evolution of scalar dissipation rate for l_{th} RIF is governed only by transient solution of $\tilde{I}_l(\mathbf{x},t)$. And the effects of each unsteady flamelet are accumulated at all the cells during the calculation. Finally, the local stationary unconditional concentrations are then computed by integration over mixture fraction, flamelet time, and summation over the number of particles :

$$\tilde{Y}_k(\mathbf{x}) = \frac{\sum_{l=1}^{N_l}\int_0^{\infty}\int_0^1 \tilde{I}_l(\mathbf{x},t)\,Y_k^l(Z,\langle\chi/Z\rangle_l;t)\,\tilde{P}(Z;\mathbf{x})\,dZ\,dt}{\sum_{l=1}^{N_l}\int_0^{\infty}\tilde{I}_l(\mathbf{x},t)\,dt} \quad (9)$$

Thus, the conditional means at a given location x can be determined as

$$\langle Y_k|Z^*=Z\rangle(Z;\mathbf{x}) = \frac{\sum_{l=1}^{N_l}\int_0^{\infty}\tilde{I}_l(\mathbf{x},t)\,Y_k^l(Z,t)\,dt}{\sum_{l=1}^{N_l}\int_0^{\infty}\tilde{I}_l(\mathbf{x},t)\,dt} \quad (10)$$

The distribution of conditional means is more critical for the model validation because the predicted conditional means are interpreted as local flame structure and are less affected by uncertainties in the local probability density function subject to mean and variance of mixture fraction. The detailed formulations of the unsteady flamelet modeling can be found elsewhere (Kim et al., 2001).

2.3 Numerical model

In order to accurately and efficiently treat the physically and geometrically complex reacting flow fields, the present study adopts the unstructured grid finite-volume method (Kang and Kim, 2003). In this unstructured-grid procedure, the conservative forms of the governing equations are integrated over a cell-centered control volume with collocated storage for all transport variables. The data connectivity is constructed based on each edge (each cell face for 3-D) since it is likely to be more effective than cell- or node point-based connectivity. In the turbulent nonpremixed jet flames investigated in this study, the high-gradient reaction zone near the mean stoichiometric line is adaptively resolved by the unstructured grid arrangement. A second-order upwind scheme for convection terms and the central differencing scheme for diffusion terms are employed. The pressure-velocity coupling is handled by SIMPLEC algorithm. More detailed information can be found elsewhere (Kang and Kim, 2003). It is well known that the standard k-ε turbulence model fails to predict correctly the complex recirculating flow. In this study, therefore, model constants of the standard k-ε turbulence model are properly modified according to the previous work (Turpin and Troyes, 2000) where the semi-empirical model constants were suggested for prediction of the turbulent axisymmetric flows.

In the solution procedure of the steady flamelet model, the flamelet equations, Eqs. (1) and (2) are discretized in mixture fraction space by finite differences and then solved using the two-point boundary value solver TWOPNT which is based on a modified damped Newton algorithm (Grcar, 1992). The combined Newton-time step method is quite reliable and fast. However this approach is not suitable for a transient problem because the time stepping procedure has a relatively poor accuracy in the temporal domain. Therefore the unsteady solution of the flamelet equations is obtained by the time integration using the stiff ODE solver, LSODE (Radhakrishnan and Hindmarsh, 1993).

3. Results and Discussions

The bluff-body combustors have been widely utilized in many engineering applications. The

experimental and theoretical researches (Roquemore et al., 1984 ; Dally et al., 1998 ; Kim et al., 2000) have been carried out for the bluff-body stabilized flows because this type of flame field has the excellent turbulent mixing characteristics and improved flame stability. Besides these practical interests, the bluff-body stabilized flames are very useful to study the interaction between turbulence and chemistry in the turbulent recirculating reactive flows. Due to its simple and well-defined boundary conditions as well as its ability to maintain the flame stabilization for a wide range of inlet conditions, the bluff-body stabilized flames are now the popular subjects for combustion laser diagnostics and modeling.

In the present study, the EPFM model has been employed to predict the flame structure and NOx formation of the methanol-air bluff-body stabilized flames for which detailed experimental data (Dally et al., 1998) are available. The burner has a bluff-body diameter, D_B=50 mm and fuel jet diameter, D_J=3.6 mm. Methanol (CH_3OH) is evaporated and delivered through a heated line, and injected at 373 K. The stoichiometric mixture fraction and the adiabatic flame temperature are 0.135 and 2260 K, respectively. The coflow air velocity is set to 40 m/s. Computations are performed for two fuel injection velocities of 80 m/s (ML1 flame) and 121 m/s (ML2 flame) which are corresponding to 55 and 84% of the blow-off velocity, respectively. The computational domain extends axially to x=300 mm ($6.0D_B$) and radially to r=100 mm ($2.0D_B$). The fully developed condition is imposed on the outlet and the free stream condition is specified at the open boundary.

Two flames investigated in this study are classified as the fuel-jet dominant flame where fuel jet with higher momentum flux continuously penetrates into the recirculation zone formed behind the flame holder and passing by the neck zone, followed by a long, jet-like flame at the further downstream region. The neck zone in the bluff-body stabilized flames is located around at the edge of the recirculation zone. In this neck zone, the turbulent mixing is intense and flame blow-off possibly occurs for sufficiently high flow velocities.

In this work, combustion of methanol-air is described by the detailed mechanism by Warnatz consisting of 82 elementary reactions with 24 species (downloadable at the IWR internet site, http ://reaflow.iwr.uni-heidelberg.de/). To predict NOx formation with the full NOx chemistry (Hewson, 1997), the 101 irreversible reactions with 13 additional species (NO, N, NO_2, NH_3, NH_2, NH, HNO, N_2H, N_2O, HNCO, NCO, HCN, CN) are added.

As previously discussed in the studies of the $CO/H_2/N_2$ jet flames (Kim et al., 2001), the mean velocity and mixture fraction fields are provided by numerical results of the steady flamelet model. In order to make the unsteady flamelet model tractable and robust, the present approach is based on an underlying assumption that, for the stationary turbulent flames, the mean density field predicted by the steady flamelet model is little influenced by the unsteady flamelet procedure. This procedure is so-called the postprocessing mode using unsteady flamelets and the main

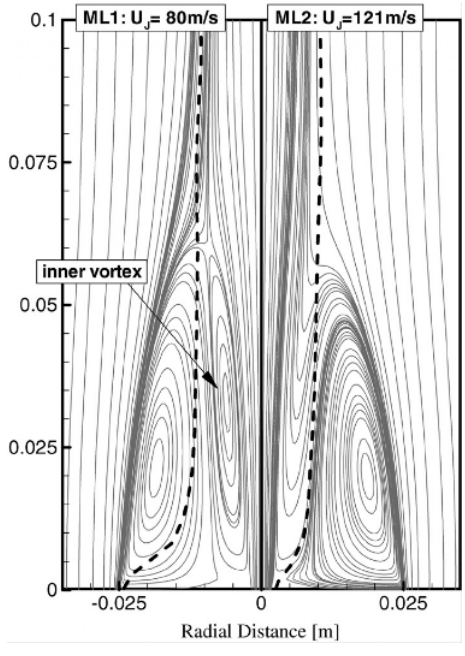

Fig. 1 Predicted steamlines for the bluff-body stabilized methanol flames with fuel jet velocities of 80 m/s (ML1, left) and 121 m/s (ML2, right) : dashed lines represent mean stoichiometry line (Z_{st}=0.135)

purpose of this treatment is to precisely predict the formation process of NOx and soot in the stationary turbulent flames. Similar idea has also been adopted in the elliptic CMC simulation (Kim et al., 2000) of bluff-body stabilized flames.

Figure 1 shows the predicted flow structures of the bluff-body burner for the fuel injection velocities of 80 m/s (ML1 flame) and 121 m/s (ML2 flame). It can be clearly seen that the quite different flow patterns are created for two flames. In case of the lower fuel-jet velocity (ML1 flame), an inner vortex near the central fuel jet is formed and the large portion of fuel is transported from the inner vortex to the outer vortex. In case of the higher fuel-jet velocity (ML2 flame), the jet momentum flux is considerably increased so that the inner vortex nearly disappears, and most of fuel penetrates along the centerline and passes downstream without being transported to the outer vortex. The stoichiometric lines represented by the dashed line characterize the different mixing pattern of two flames. The stoichiometric line of the ML1 flame is placed along the edge of the outer vortex whereas that of the ML2 flame is located along the edge of the central fuel jet. Consequently, the corresponding flame structure of two flames becomes quite different in the proximity of the outer core vortex zone.

In the framework of the present EPFM model, 10 RIFs are used to account for spatially distributed inhomogeneity of scalar dissipation rate. Fig. 2 presents the temporal history of total mass within the computational domain and the conditional dissipation rate for each RIF. The scalar dissipation rate remains relatively high and does not decrease so rapidly as that of downstream

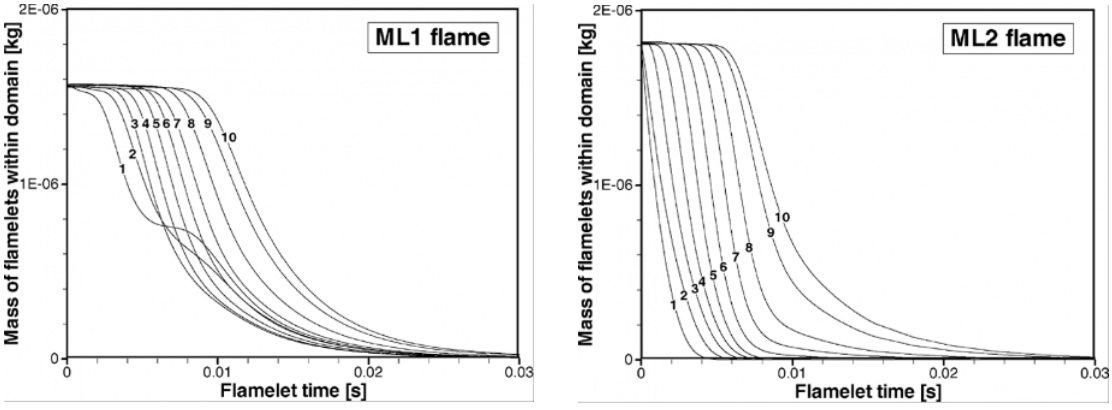

(a) Mass of flamelets within computational domain

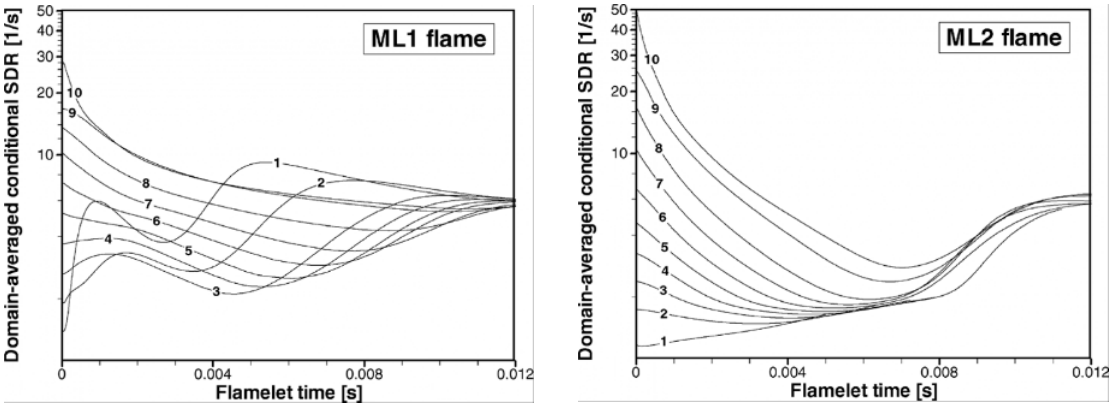

(b) Domain-averaged conditional scalar dissipation rate

Fig. 2 Temporal history of total mass of flamelets within computational domain and the domain-averaged conditional scalar dissipation rates

region of the jet flames. For the ML2 flame with higher fuel jet velocity, RIFs leave more quickly the computational domain through the exit boundary and initial levels of scalar dissipation rate are slightly higher than those of the ML1 flame. The presence of inner vortex and fuel-rich mixtures within the outer vortex makes some RIF to undergo more complex temporal change of scalar dissipation rate.

In Fig. 3, radial profiles of mean and rms mix-

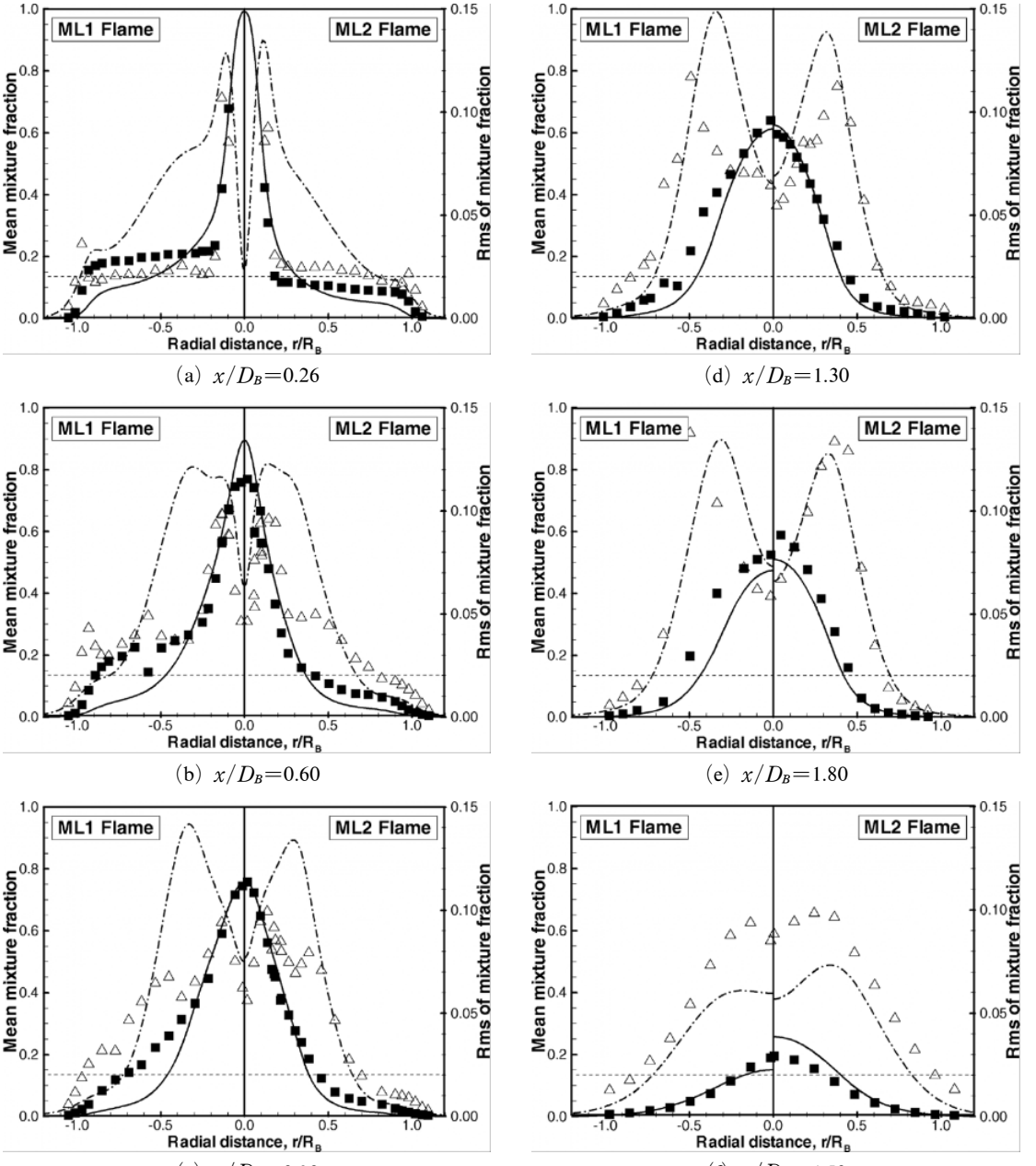

Fig. 3 Radial profiles of mean (solid line, square) and rms (dashdot line, triangle) of mixture fraction for the bluff-body stabilized methanol flames with fuel jet velocities of 80 m/s (ML1, left) and 121 m/s (ML2, right)

ture fraction are presented at six different axial locations. The noticeable difference in the mixing characteristics of two flames, as discussed above, exists at the recirculation zone. Experimental data at $x/D_B=0.26$ indicates that the outer vortex has a nearly uniform distribution of mean mixture fraction for both flames.

In term of the mixture status in the upstream outer vortex region, the ML1 flame yields the slightly fuel-rich mixtures whereas the ML2 flame does the slightly fuel-lean mixtures. However, in the outer vortex region of both flames, there exist the large differences between prediction and measurement in terms of the level and uniformity of mean mixture fraction. The level of mean mixture fraction is significantly underpredicted and its rms level is overestimated. The overestimated rms value of mean mixture fraction leads to the overprediction of mixtutre fraction fluctuation in the same region. These discrepancies are relatively pronounced for the ML1 flame and the relatively large deviations are also found in the downstream recirculation zones ($x/D_B=0.6$, 0.9). At the further downstream regions ($x/D_B>1.3$), the mixture fraction fields of two flames become gradually similar and the differences between prediction and measurement noticeably decrease.

Figure 4 presents the radial profiles of mean temperature and OH mass fraction at the six axial locations. Experimental profiles indicate that the outer-vortex reaction zone represented by peaks of mean temperature and OH mass fraction are quite different for two flames. As shown in experimental results of recirculation zone ($x/D_B=$ 0.26, 0.6, and 0.9), the ML1 flame creates the peak temperature and maximum OH zone at the air side edge of the outer vortex because the mean mixtures of the outer vortex are uniformly fuel-rich and become stoichiometric only on its air-side edge. In the ML2 flame, on the other hand, the reaction zone with the maximum temperature and OH distribution is located close to the shear layer between outer vortex and central fuel jet where the stoichiometric mean mixture is formed. However, the numerical model fails to correctly capture the flame structure of outer vortex in the ML1 flame due to the inaccurate prediction of mixture fraction field. The present model predicts the much higher and broader distribution of OH mass fraction in the outer vortex region since the predicted mean mixture fraction in this region is relatively close to stoichiometry. For the same region of the ML2 flame, however, numerical results are relatively well agreed with experimental data in terms of mean OH mass fraction although mean temperature is still underestimated due to the underpredicted mean mixture fraction and the overestimated fluctuation. After passing the neck zone, as shown in Fig. 4(e), the mean temperature for two flames significantly decreases due to the intense mixing.

Figure 5 shows the radial profiles of mean mass fraction of NO for two flames. Nevertheless of the inaccurately predicted mixing pattern within the outer vortex, the present approach predicts the mean mass fraction of NO with the acceptable level. In the outer vortex of the ML1 flame, the substantial amount of NO is formed due to the presence of visible flame within this region. On the other hand, for the ML2 flame, the NO level produced in the combustion zone is relatively low because the stoichiometric mixtures are placed around at the shear layer of the inner zone and the inner zone allows the much shorter residence times than does the outer vortex zone. As pointed out in the experimental work of Dally et al.(1996), the level of NO produced in the recirculation zone decreases or remains constant within the neck zone and gradually increases with the axial distance at the further downstream region. These qualitative trends are well predicted by the present model even if the overall NO levels are overestimated for both flames. This will be precisely discussed later in terms of the conditional means.

Figure 6 shows the conditional means of temperature and OH mass fraction at three different axial locations of $x/D_B=0.6$, 1.3, and 4.5. The scatter plots represent the instantaneous measured data near the same radial position and the predicted conditional means are obtained at $r=3D_J$, where D_J is the fuel nozzle diameter. For comparative purpose, the equilibrium limits denoted by the dashdot lines are also presented. The

equilibrium chemistry usually leads to the unacceptable results for the hydrocarbon combustion processes because the CO consumption rates are slow especially for the very fuel-rich mixtures with the low temperature which is unlikely to reach the chemical equilibrium state. Therefore, the equilibrium limits are obtained not by the chemical equilibrium solution but by the steady flamelet solution at a very small scalar dissipation rate, i.e. 0.001 sec^{-1}.

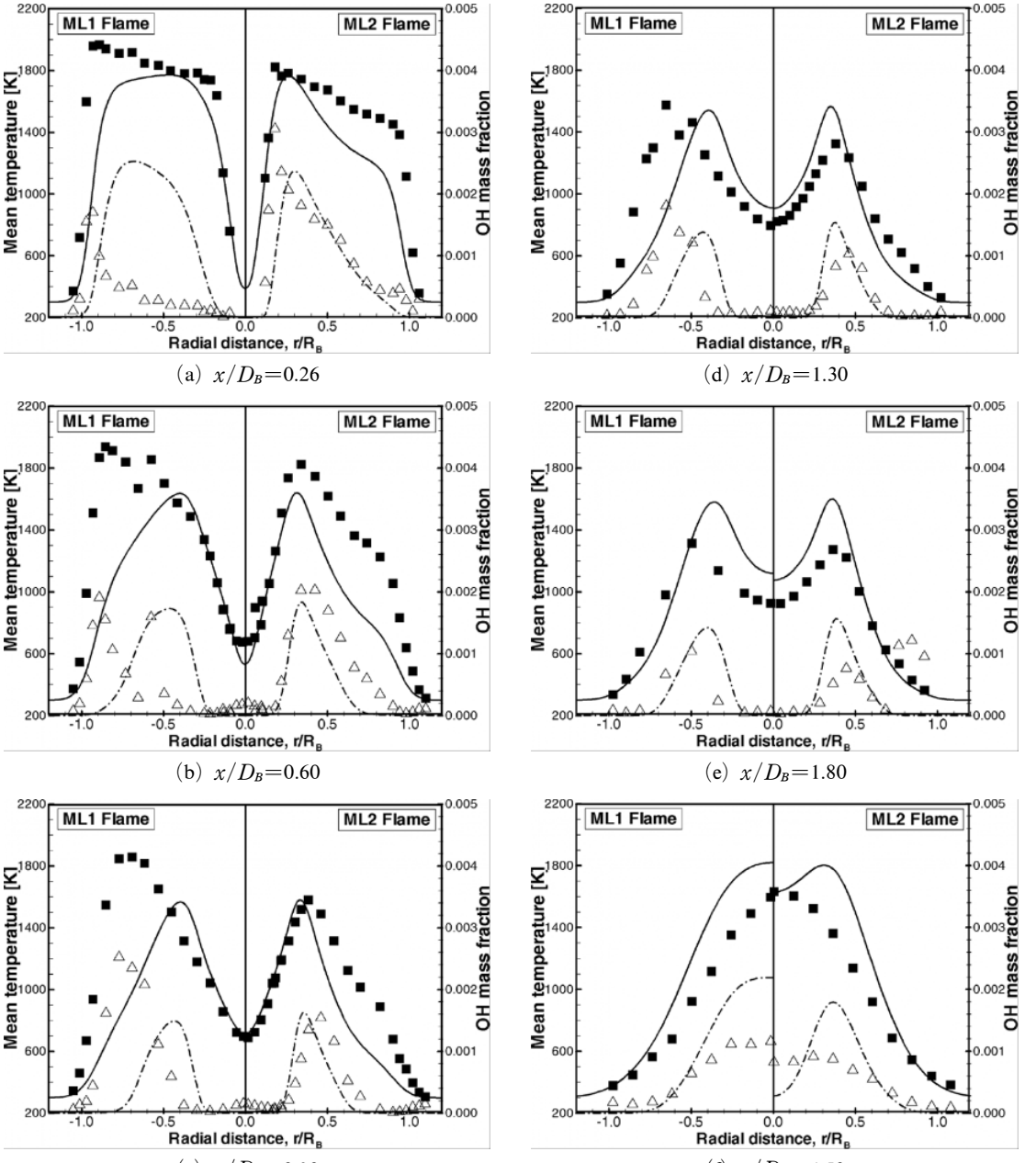

Fig. 4 Radial profiles of mean temperature (solid line, square) and OH mass fraction (dashdot line, triangle) for the bluff-body stabilized methanol flames with fuel jet velocities of 80 m/s (ML1, left) and 121 m/s (ML2, right)

At upstream region within the recirculation zone (x/D_B=0.6), the predicted peak values of temperature and OH are 1988 K and 0.518% for the ML1 flame, and 1972 K and 0.535% for the ML2 flame, respectively. Compared to the equilibrium limit, the predicted OH level clearly reveals that the superequilibrium concentrations of radicals are substantially appeared in this region since the third-body recombination reactions of radical pools become much slower due to the locally insufficient residence time and the intense turbulent mixing. At the further downstream re-

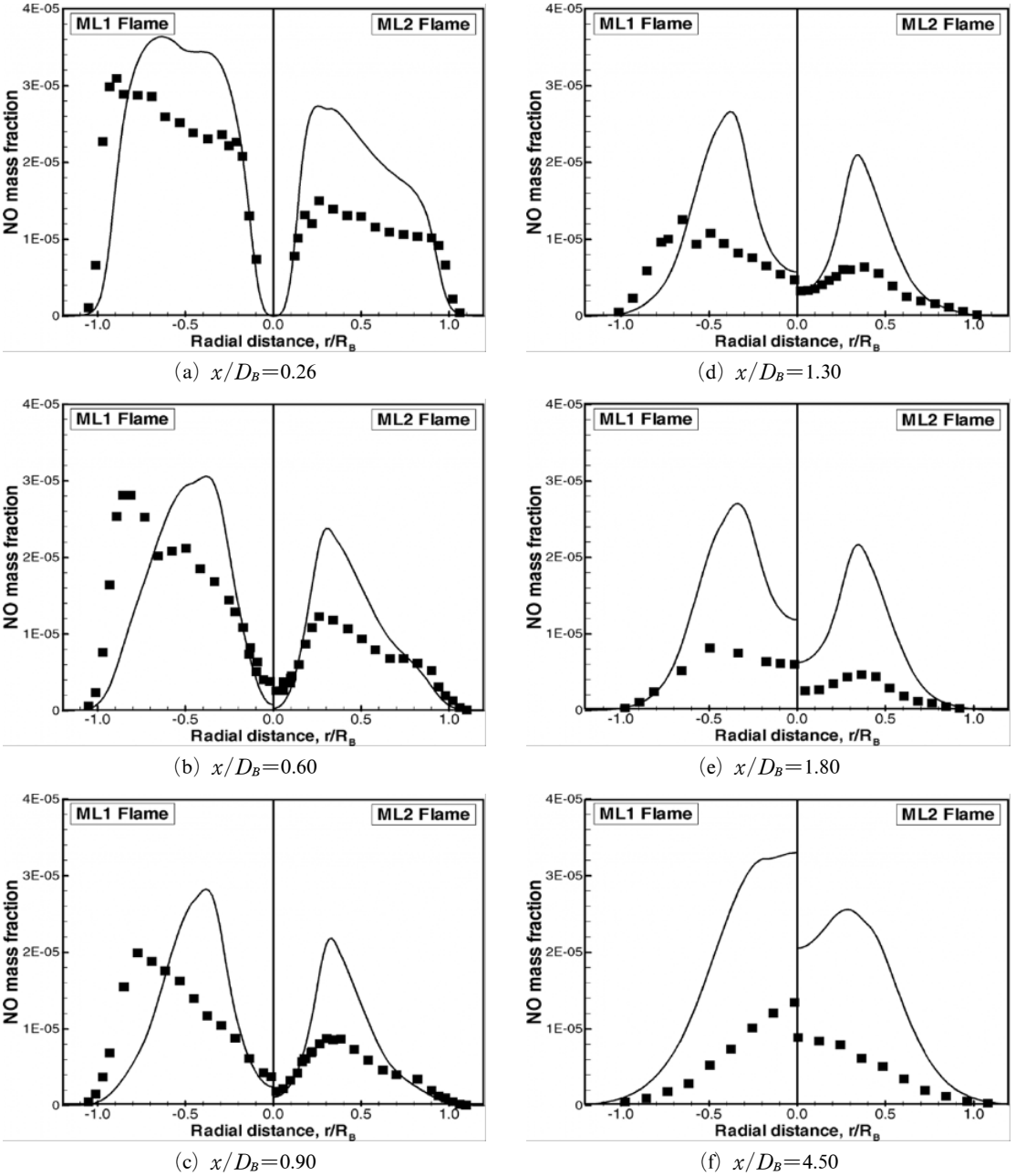

(a) x/D_B=0.26 (d) x/D_B=1.30

(b) x/D_B=0.60 (e) x/D_B=1.80

(c) x/D_B=0.90 (f) x/D_B=4.50

Fig. 5 Radial profiles of mean mass fractions of NO for the bluff-body stabilized methanol flames with fuel jet velocities of 80 m/s (ML1, left) and 121 m/s (ML2, right)

gion (x/D_B=4.5), the peak temperature increases up to 2028 K and 2058 K for the ML1 and the ML2 flames, respectively while the peak values of OH mass fraction decrease slightly to 0.468% (ML1) and 0.454% (ML2). The downstream decaying behavior to the equilibrium state is slightly different for two flames owing to the different temporal history of conditional scalar dissipation rate shown in Fig. 2.

For the ML2 flame, the predicted results of conditional means are quite consistent with the experimental observation (Dally et al., 1998) that the peak OH mass fraction has decreased slightly from 0.58% at x/D_B=0.6 to 0.48% at x/D_B=4.5

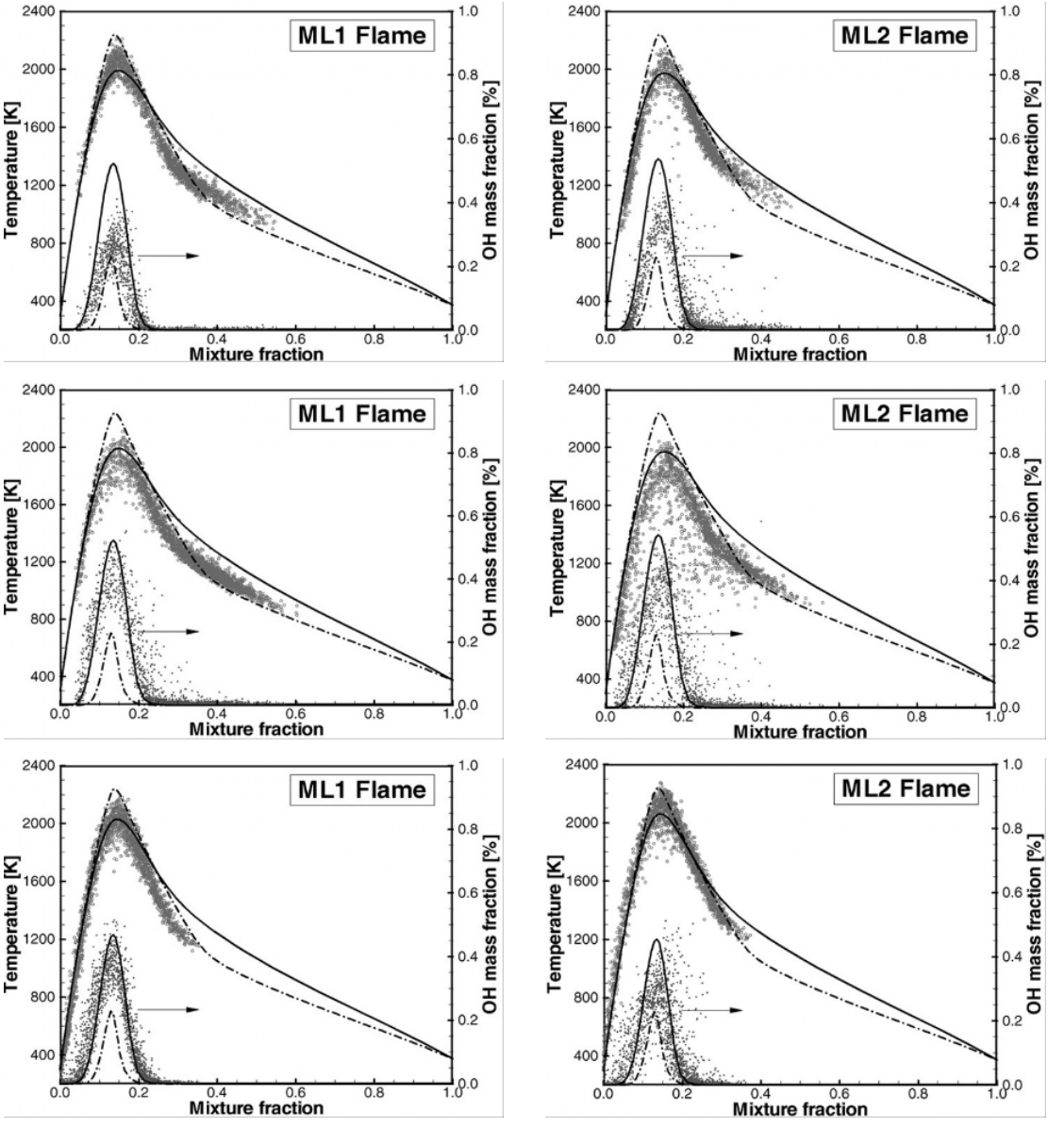

Fig. 6 Comparison of conditional means of temperature and OH mass fraction for fuel jet velocities of 80 m/s (ML1, left column) and 121 m/s (ML2, right column) at X/D_B=0.6 (top), 1.3 (middle) and 4.5 (bottom) : solid line (EPFM model) ; dashed dot (steady flamelet solution at χ_{st}=0.001 sec^{-1}) ; scatter plots (measurement)

while the peak temperature has increased approximately by 80 K. At the neck zone (x/D_B=1.3), the predicted maximum conditional means of temperature and OH mass fraction are 1985 K and 0.518 for the ML1 flame, and 1970 K and 0.542 for the ML2 flame. In terms of the maximum OH mass fraction, at the neck zone of the ML2 flame, the predicted value (0.542%) is slightly lower than

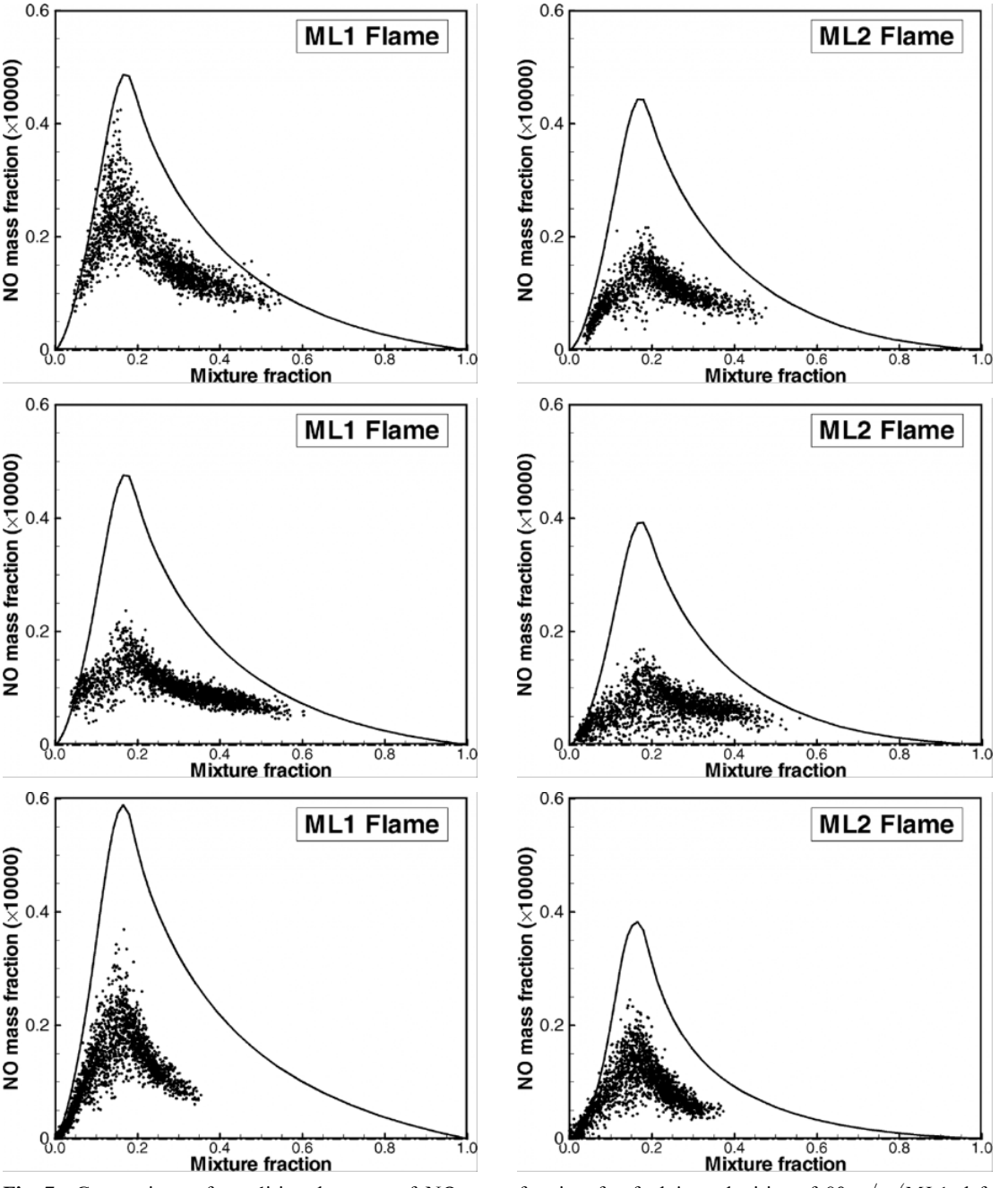

Fig. 7 Comparison of conditional means of NO mass fraction for fuel jet velocities of 80 m/s (ML1, left column) and 121 m/s (ML2, right column) at X/D_B=0.6 (top), 1.3 (middle) and 4.5 (bottom) : solid line (EPFM model) ; scatter plots (measurement)

the measured one (0.6%). Experimental data of the ML2 flame in the neck zone indicate that the certain portion of mixture particles is locally extinguished or partially burnt at the given fuel jet velocity (121 m/s) which is 84% of the blow-off velocity. However, when the relatively small fraction of mixture particles is locally extinguished, numerical results indicate that the present EPFM model still predicts the acceptable distribution of conditional means of temperature and OH mass fraction even if it is unable to capture the whole physics associated with the local extinction.

Figure 7 displays the conditional means of NO mass fraction at three axial locations for two flames. In comparison with measurement, the overall NO levels obtained by the present model are overestimated. The predicted NO levels of the ML2 flame are lower than those of the ML1 flame due to the higher fuel jet velocity and the shorter residence time.

According to experimental results (Dally et al., 1996) of the ML1 flame, the peak NO mole fraction drops from 50 to 20 ppm as the axial location increases from $x/D_B=0.26$ to 1.8, and then increases up to roughly 40 ppm at the further downstream region. For the ML2 flame, the measured peak NO mass fraction decreases from about 20 ppm at $x/D_B=0.6$ to approximately 16 ppm at $x/D_B=1.3$ (Dally et al., 1996). In experimental work, it is also suggested that the decrease of NO level observed in the neck zone could be attributed to the considerable decrease in NO production and might be associated with the conversion process of NO to N2 which is enhanced by the relatively high fuel concentration.

In case of the ML1 flame, the decrease of the peak NO level near the neck zone is also identified even with unnoticeably small amount and then the peak NO level increases with the axial distance at the further downstream region. Since the present NOx chemistry involves the reaction paths by NOx reburn (Hewson, 1997), numerical results potentially reflect the conversion of NO to N2 by the hydrocarbon radicals formed in the fuel-rich mixtures. Thus, it is quite desirable that one of further detailed study is focused on this subject.

4. Conclusions

In order to assess the capability of the EPFM model to predict the flame structure and NOx formation in the multi-dimensional elliptic turbulent flame field, the methanol-air bluff-body flames have been numerically investigated for two different fuel jet velocities. Based on numerical results obtained in the present study, the following conclusions can be drawn:

(1) In case of the higher fuel jet velocity (120 m/s), numerical results are reasonably well agreed with experimental data. However, in case of the lower fuel jet velocity (80 m/s), there exist the considerable qualitative and quantitative differences between prediction and measurement especially at the recirculation zone close to inlet. These discrepancies might be attributed mainly to the defect of the modified k-ε turbulence model to predict incorrectly the mixture fraction field as well as partly to the limitation of the present turbulent combustion model to deal with the relatively thick flame zone and the partially premixed flame fields. Nevertheless of these deviations, numerical results suggest that the present EPFM model has the predicative capability to realistically capture the essential features of flame structure and NOx formation in the bluff-body stabilized flames.

(2) In term of the mixture status in the upstream outer vortex region, the ML1 flame yields the slightly fuel-rich mixtures whereas the ML2 flame does the slightly fuel-lean mixtures. However, in the outer vortex region of both flames, there exist the large differences between prediction and measurement in terms of the level and uniformity of mean mixture fraction. The level of mean mixture fraction is significantly underpredicted and its rms level is overestimated. These discrepancies are relatively pronounced for the ML1 flame and the relatively large deviations are also found in the upstream recirculation zones ($x/D_B=0.6$, 0.9). At the further downstream regions ($x/D_B>1.3$), the mixture fraction fields of two flames become gradually similar and the

differences between prediction and measurement noticeably decrease.

(3) For the ML2 flame, the predicted results for conditional means of temperature and OH mass fraction are generally consistent with the experimental profiles. In terms of the maximum OH mass fraction, at the neck zone of the ML2 flame, the predicted value (0.542%) is slightly lower than the measured one (0.6%). Experimental data of the ML2 flame in the neck zone indicate that the certain portion of mixture particles is locally extinguished or partially burnt at the given fuel jet velocity (121 m/s). However, for these methanol flames where the relatively small fraction of mixture particles is locally extinguished, numerical results indicate that the present EPFM model still predicts the acceptable distribution of conditional means of temperature and OH mass fraction even if it is unable to capture the whole physics associated the local extinguished combustion processes.

(4) In comparison with measurement, the overall NO levels obtained by the present model are overestimated. The predicted NO levels of the ML2 flame are lower than those of the ML1 flame due to the higher fuel jet velocity and the shorter residence time. Numerical results potentially reflect the conversion of NO to N2 by the hydrocarbon radicals formed in the fuel rich mixture near the neck zone and further detailed study on this subject needs to be carried out.

References

Barths, H., Hasse, C., Bikas, G. and Peters, N., 2000, "Simulation of Combustion in Direct Injection Diesel Engines Using an Eulerian particle Flamelet Model," *Proc. 28th Symp.(Int.) Comb.*, Combustion Institute, Pittsburgh, pp. 1161~1168.

Barths, H., Peters, N., Brehm, N., Mack, A., Pfitzner, M. and Smiljanovski, V., 1998, "Simulation of Pollutant Formation in a Gas-Turbine Combustor using Unsteady Flamelets," *Proc. 27th Symp.(Int.) Comb.*, Combustion Institute, Pittsburgh, pp. 1841~1847.

Chen, M., Herrmann, M. and Peters, N., 2000, "Flamelet Modeling of Lifted Turbulent Methane/Air and Propane/Air Jet Diffusion Flames," *Proc. 28th Symp.(Int.) Comb.*, Combustion Institute, Pittsburgh, pp. 167~174.

Coelho, P. J. and Peters, N., 2001, "Numerical Simulation of a MILD Combustion Burner," *Combustion and Flame*, Vol. 124, pp. 503~518.

Dally, B. B., Masri, A. R., Barlow, R. S., Fiechtner, G. J. and Fletcher, D. F., 1996, "Measurements of NO in Turbulent Non-premixed Flames Stabilized on a Bluff Body," *Proc. 26th Symp.(Int.) Comb.*, Combustion Institute, Pittsburgh, pp. 2191-2197.

Dally, B. B., Masri, A. R., Barlow, R. S. and Fiechtner, G. J., 1998, "Instantaneous and Mean Compositional Structure of Bluff-Body Stabilized Nonpremixed Flames," *Combustion and Flame*, Vol. 114, pp. 119~148.

Ferreira, J. C., 1996, *Flamelet Modelling of Stabilization in Turbulent Non-premixed Combustion*, PhD Thesis, ETHZ Zuerich Switzerland.

Grcar, J.F., 1992, *The Twopnt Program for Boundary Value Problems*, Sandia Report, SAND91-8320, Livermore.

Hewson, J. C., 1997, *Pollutant Emissions from Nonpremixed Hydrocarbon Flames*, PhD Thesis, University of California, San Diego.

Kang, S. M. and Kim, Y. M., 2003, "Parallel Unstructured-Grid Finite-Volume Method for Turbulent Nonpremixed Flames Using the Flamelet Model," *Numerical Heat Transfer*, Part B, Vol. 43, pp. 525~547.

Kim, H. J. and Kim, Y. M., 2002, "Numerical Modeling for Combustion and Soot Formation Processes in Turbulent Diffusion Flames," *KSME Int. J.*, Vol. 16, No. 1, pp. 116~124.

Kim, H. J., Kim, Y. M. and Ahn, K. Y., 2004a, "Numerical Modeling of Turbulent Nonpremixed Lifted Flames," *KSME Int. J.*, Vol. 18, No. 1, pp. 167~172.

Kim, S. H., Huh, K. Y. and Tao, L., 2000, "Application of the Elliptic Conditional Moment Closure Model to a Two-Dimensional Nonpremixed Methanol Bluff-Body Flame," *Combustion and Flame*, Vol. 120, pp. 75~90.

Kim, S. K., Kang, S. M. and Kim, Y. M., 2001, "Flamelet Modeling for Combustion Processes and NOx Formation in the Turbulent Nonpremexed $CO/H_2/N_2$ Jet Flames," *Combustion Sci-*

ence and Technology, Vol. 168, pp. 47～83.

Kim, S. K., Yu, Y., Ahn, J. and Kim, Y. M., 2004b, "Numerical Investigation of the Autoignition of Turbulent Gaseous Jets in a High-Pressure Environment Using the Multiple-RIF Model," *Fuel*, Vol. 83, pp. 375～386.

Klimenko, A. Y. and Bilger, R. W., 1999, "Conditional Moment Closure for Turbulent Combustion," *Prog. Energy Combust. Sci*., Vol. 25, pp. 595～687.

Kronenburg, A., Bilger, R. W. and Kent, J. H., 2000, "Computation of Conditional Average Scalar Dissipation in Turbulent Jet Diffusion Flames," *Flow, Turbulence and Combustion*, Vol. 64, pp. 145～159.

Libby, P. A. and Williams, F. A., eds, 1994, *Turbulent Reacting Flows*, New York, Academic Press.

Marracino, B. and Lentini, D., 1997, "Radiation Modelling in Non-Luminous Nonpremixed Turbulent Flames," *Combustion Science and Technology*, Vol. 128, p. 23.

Peters, N., 1986, "Laminar Flamelet Concepts in Turbulent Combustion," *Proc. 21st Symp.(Int.) Comb*., Combustion Institute, Pittsburgh, pp.1231～1250.

Peters, N., 2000, *Turbulent Combustion*, Cambridge University Press.

Pitsch, H. and Steiner, H., 2000, "Large-Eddy Simulation of a Turbulent Piloted Methane/Air Diffusion Flame (Sandia Flame D)," *Physics of Fluids*, Vol. 12, pp. 2541～2554.

Pitsch, H., 2000, "Unsteady Flamelet Modeling of Differential Diffusion in Turbulent Jet Diffusion Flames," *Combustion and Flame*, Vol. 123, pp. 358～374.

Pitsch, H., Barths, H. and Peters, N., 1996, "Three-Dimensional Modeling of NOx and Soot Formation in DI-Diesel Engines Using Detailed Chemistry Based on the Interactive Flamelet Approach," SAE paper 962057.

Pitsch, H., Chen, M. and Peters, N., 1998, "Unsteady Flamelet Modeling of Turbulent Hydrogen-Air Diffusion Flames," *Proc. 27th Symp. (Int.) Comb*., Combustion Institute, Pittsburgh, pp. 1057～1064.

Pitsch, H., Riesmeier, E. and Peters, N., 2000, "Unsteady Flamelet Modeling of Soot Formation in Turbulent Jet Diffusion Flames," *Combustion Science and Technology*, Vol. 158, pp. 389～406.

Pope, S. B., 2000, *Turbulent Flows*, Cambridge University Press.

Radhakrishnan, K. and Hindmarsh, A. C., 1993, "Description and Use of LSODE, the Livermore Solver for Ordinary Differential Equations," *Lawrence Livermore National Laboratory Report*, UCRL-ID-113855.

Roquemore, W. M., Tankin, R. S., Chiu, H. H. and Lottes, S. A., 1984, "The Role of Vortex Shedding in a Bluff-Body Combustor," *Experimental Measurement and Techniques in Turbulent Reactive and Nonreactive Flows*, Vol. 66, pp. 159～174.

Turpin, G. and Troyes, J., 2000, "Validation of a Two-Equation Turbulence Model for Axisymmetric Reacting and Nonreacting Flows," AIAA paper 2000-3463.

Vervisch, L. and Veynante, D., 2002, "Turbulent Combustion Modeling," *Prog. Energy Combust. Sci*., Vol. 28, pp. 193～266.